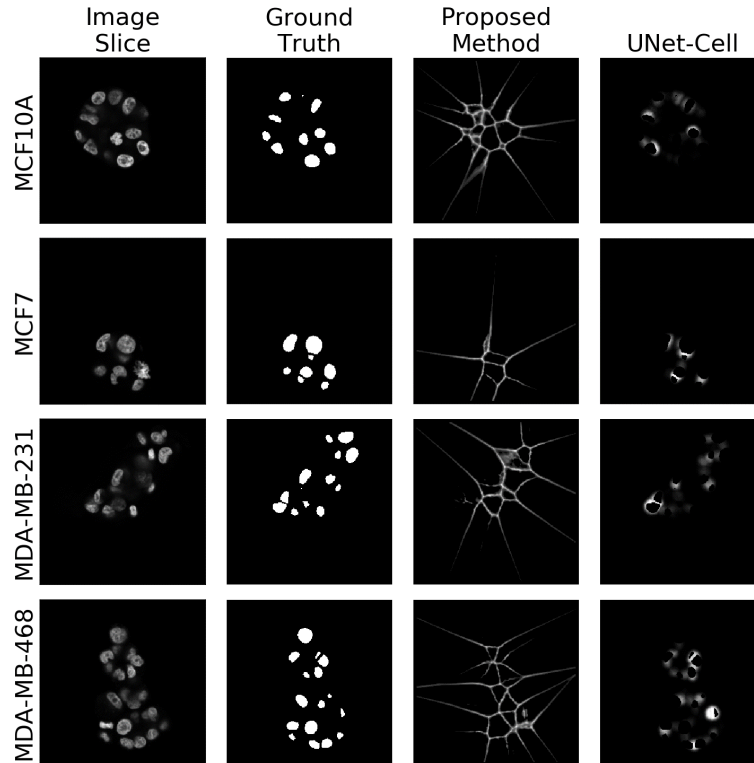


## Supplementary Section

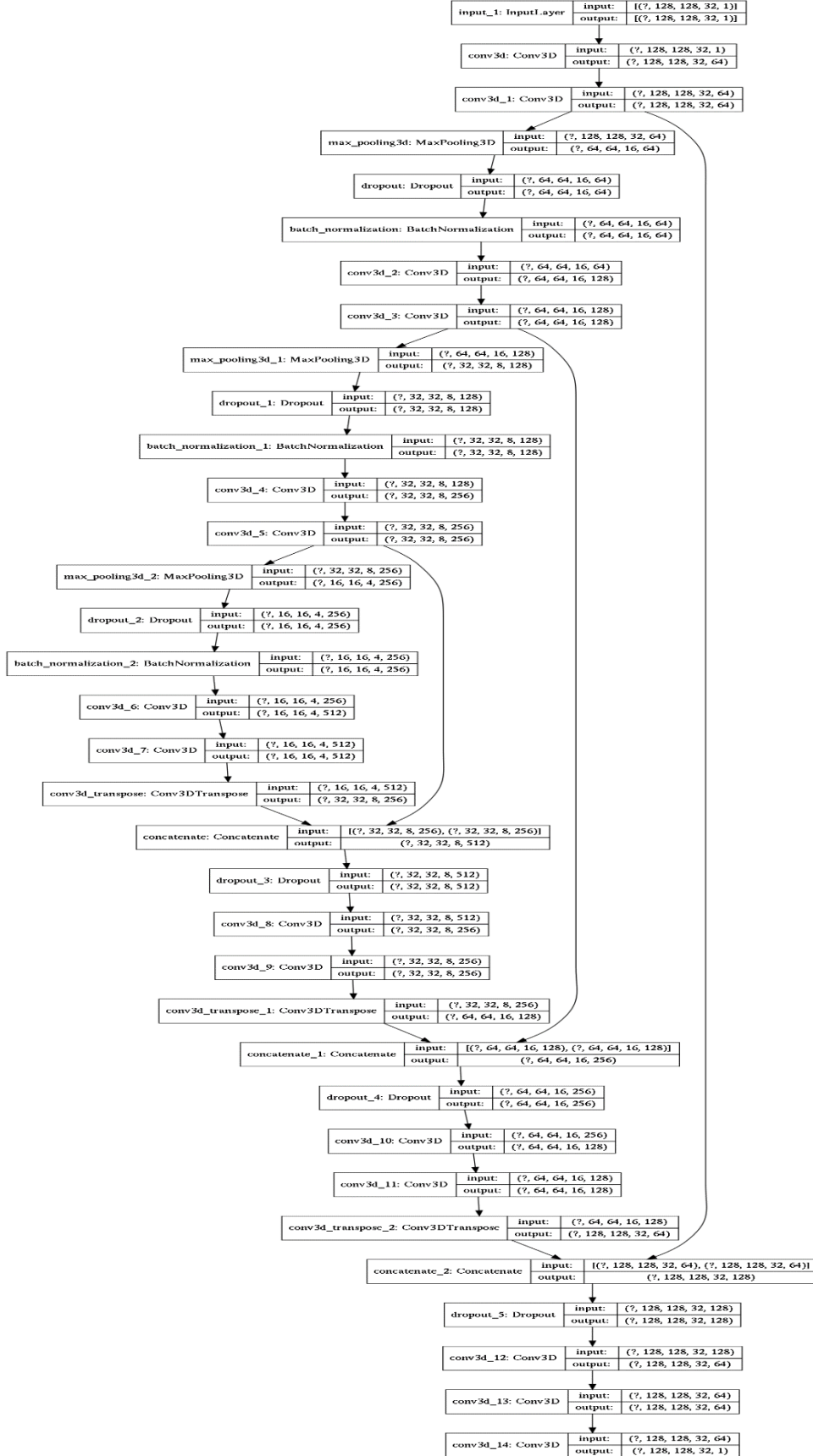
Additional information is provided for the formulation of the potential field, formulation of colony morphology (e.g., roundness, number of cells) indices, hyperparameter tuning, and visual examples of intermediate results.

### A. Potential Field

Ground truth masks are binary images with values of one indicating a nuclei and values of zero indicating background. The distance transform (DT), applied to the binary mask, computes the distance of a background pixel to the nearest nuclei pixel. This computation naturally forms local peaks at the perceptual boundary between adjacent nuclei. The second derivative of the DT is computed using a Laplacian of Gaussian (LoG) filter as multiple scales, e.g. 1, 1.5, 2, where negative values are kept, and the rest discarded. The final potential field is the minimum projection of these filter responses. Additionally, the original UNet (UNet-Cell) potential field was extended to 3D for use with this dataset. Both of these potential fields are visualized in **Supplementary Figure 1** for each cell line via middle-slice 2D views. Finally, the UNet architecture extended to 3D is shown in **Supplementary Figure 2**.



**Supplementary Figure 1:** Middle slice views of cell line images, ground truth, proposed weight map, and original weight map visualizing the differences between pixel weighting.



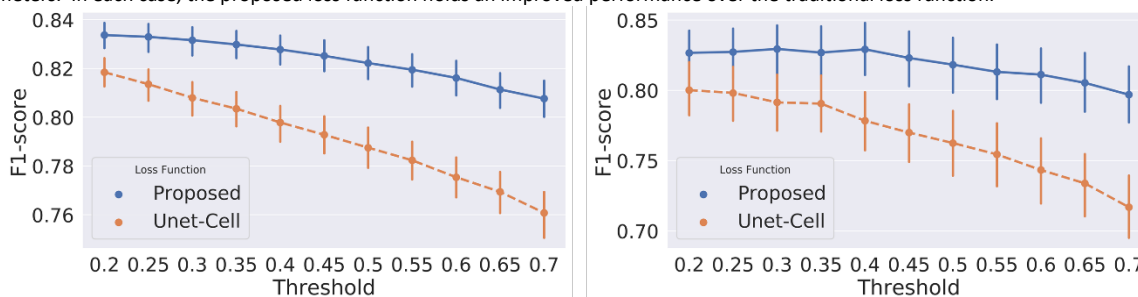
Supplementary Figure 2: UNet architecture extended to three dimensions.

## B. Computed indices for the colony morphology

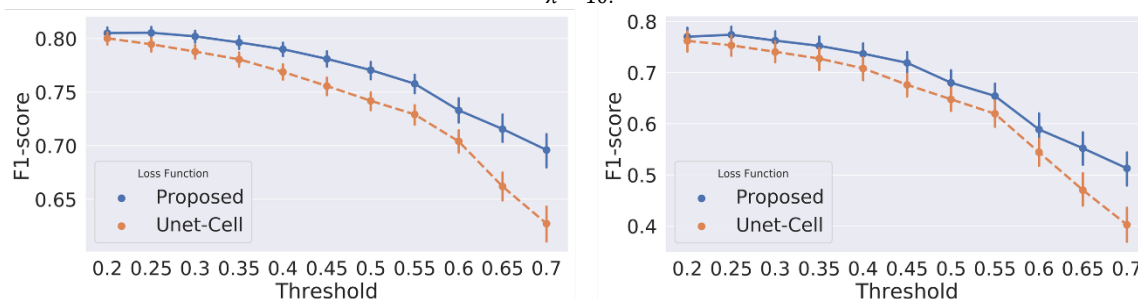
For the purpose of generating a comprehensive analysis report, several indices are computed that correspond to the proliferation rate (e.g., number of cells per colony), dysplasia and morphogenesis (e.g., shape of colony in terms of flatness, elongation, roundness), and organization and lumen formation (e.g., distribution of cells with respect to the convex hull and centroid of colony, density of colony as measured by the ratio of convex hull of a colony to the volume of all nuclei in the colony). [The details of computed morphometric indices can be found in \(Bilgin, et al., 2016\).](#)

## C. Hyperparameter tuning.

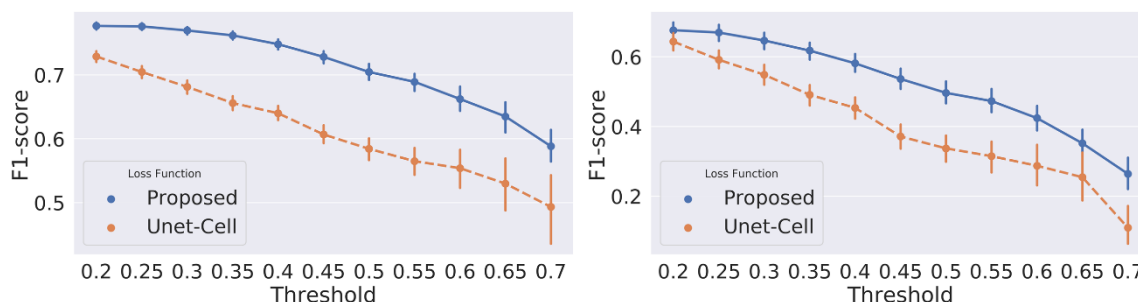
Tuning was performed for each of free variables that include the regularization parameter  $\lambda$  and the probability threshold. **Supplementary Figures 3-5** show the performance of proposed and traditional loss functions as a function of the probability threshold for different regularization parameters. In each case, the proposed loss function holds an improved performance over the traditional loss function.



**Supplementary Figure 3:** F1-score for pixel (left) and object (right) level detection as a function of probability threshold for scaling coefficient  $\lambda = 10$ .



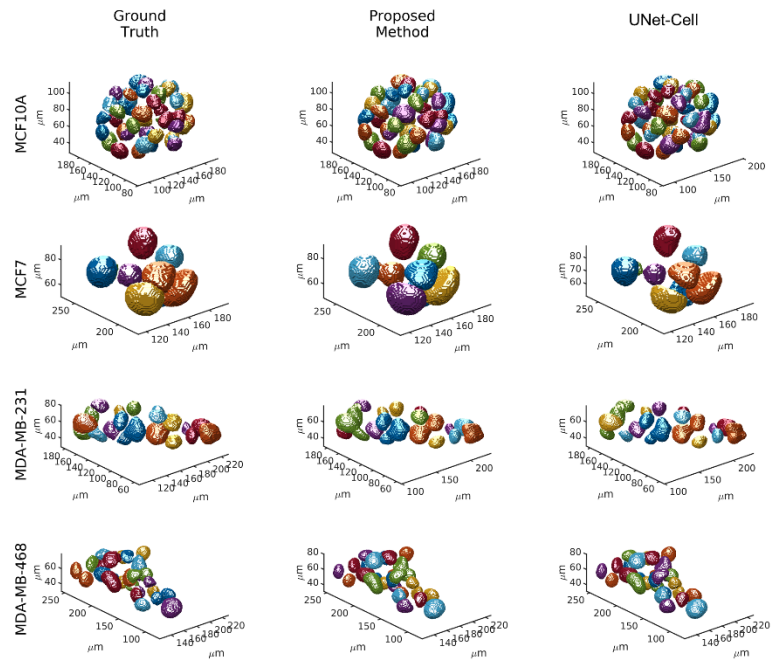
**Supplementary Figure 4:** F1-score for pixel (left) and object (right) level detection as a function of probability threshold for scaling coefficient  $\lambda = 20$ .



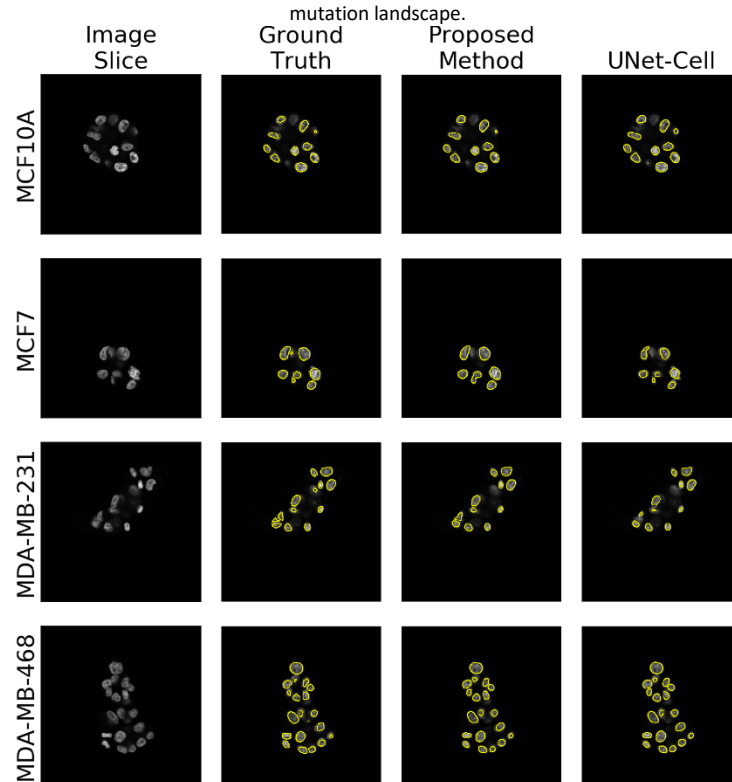
**Supplementary Figure 5:** F1-score for pixel (left) and object (right) level detection as a function of probability threshold for scaling coefficient  $\lambda = 100$ .

## D. Visual Examples of intermediate results

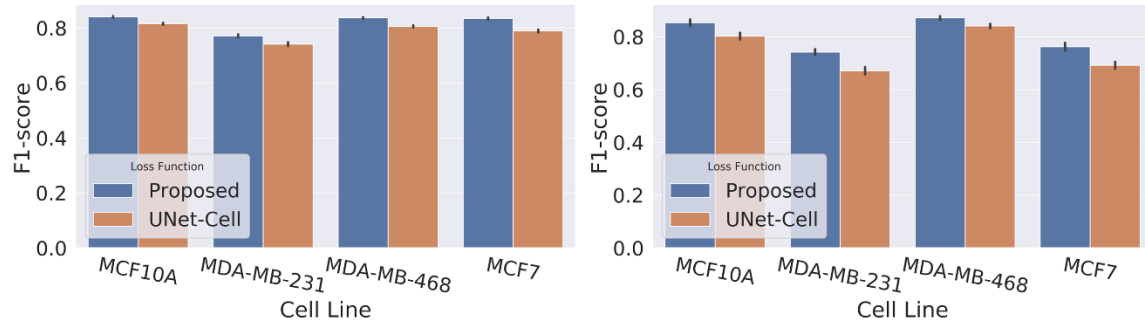
Additional visual examples are shown in **Supplementary Figures 6 and 7** for 2D slides and 3D stacks, respectively. Examples of 2D slices are selected as the middle slice view of a 3D stack, and are used to visualize pixel-level detection. 3D stacks show object-level detection and the delineation of neighboring nuclei shown in false color corresponding to uniquely labeled cells. Final predictions in both 2D and 3D are visualized with the probability threshold fixed at 0.3. Additionally, **Supplementary Figure 8** shows the robustness of model performance to variations in cell line mutations.



**Supplementary Figure 6:** 3D examples of model prediction shown with ground truths to visualize object level detection as a function of mutation landscape.



**Supplementary Figure 7:** Middle slices of cell line images with overlaid ground truth, proposed- and original-loss function predictions visualizing pixel performance of each model.



**Supplementary Figure 8:** F1-score for pixel (left) and object (right) with 95% confidence intervals as a function of cell line shows a robustness to different cancer mutations.

## External Files

The source code and training and annotated images are provided at <https://osf.io/g9xv8>.

## References

Bilgin, C.C., *et al.* BioSig3D: High content screening of three-Dimensional cell culture models. *PLoS One* 2016;11(3):e0148379.